

Phase diagram of superconductivity and antiferromagnetism in single crystals of $\text{Sr}(\text{Fe}_{1-x}\text{Co}_x)_2\text{As}_2$ and $\text{Sr}_{1-y}\text{Eu}_y(\text{Fe}_{0.88}\text{Co}_{0.12})_2\text{As}_2$

Rongwei Hu, Sergey L. Bud'ko, Warren E. Straszheim, Paul C. Canfield

Ames Laboratory, U.S. DOE and Department of Physics and Astronomy, Iowa State University, Ames, IA 50011, USA

(Dated: February 16, 2022)

We report magnetic susceptibility, resistivity and heat capacity measurements on single crystals of the $\text{Sr}(\text{Fe}_{1-x}\text{Co}_x)_2\text{As}_2$ and $\text{Sr}_{1-y}\text{Eu}_y(\text{Fe}_{0.88}\text{Co}_{0.12})_2\text{As}_2$ series. The optimal Co concentration for superconductivity in $\text{Sr}(\text{Fe}_{1-x}\text{Co}_x)_2\text{As}_2$ is determined to be $x \sim 0.12$. Based on this we grew members of the $\text{Sr}_{1-y}\text{Eu}_y(\text{Fe}_{0.88}\text{Co}_{0.12})_2\text{As}_2$ series so as to examine the effects of well defined, local magnetic moments, on the superconducting state. We show that superconductivity is gradually suppressed by paramagnetic Eu^{2+} doping and coexists with antiferromagnetic ordering of Eu^{2+} as long as $T_c > T_N$. For $y \geq 0.65$, T_N crosses T_c and the superconducting ground state (as manifested by zero resistivity) abruptly disappears with evidence for competition between superconductivity and local moment antiferromagnetism for y up to 0.72. It is speculated that the suppression of the antiferromagnetic fluctuations of Fe sublattice by coupling to the long range order of Eu^{2+} sublattice destroys bulk superconductivity when $T_N > T_c$.

PACS numbers: 74.25.Dw, 74.25.Fy, 74.25.Ha, 74.62.Dh

I. INTRODUCTION

The interplay between superconductivity (SC) and magnetism has been of a long standing interest in condensed matter physics. SC and magnetism were originally considered to be mutually exclusive in conventional superconductors because magnetism breaks the time reversal symmetry of the singlet Cooper pairs. The influence of paramagnetic impurities on SC was first studied theoretically by Abrikosov and Gor'kov (AG).¹ It was shown that SC is drastically suppressed by dilute magnetic moments due to the spin-flip scattering. Early experimental investigations were limited to superconducting systems without long-range magnetic order.²⁻⁴ The coexistence of SC and long-range magnetism was realized in several families of ternary and quaternary rare-earth compounds discovered later, also referred to as magnetic superconductors, e.g. RMO_6S_8 , RRh_4B_4 and $\text{RNi}_2\text{B}_2\text{C}$.⁵⁻¹¹ In these compounds, the localized $4f$ electrons of the rare-earth ions are indirectly coupled via conduction electrons by the Ruderman-Kittel-Kasuya-Yosida interaction (RKKY) and responsible for various magnetic orderings. The conduction electrons, often primarily from the transition metal, give rise to SC. The coexistence is more favorable for antiferromagnetism (AF), since the AF molecular field exerted on SC electrons may be averaged out on the scale of SC coherence length.

Another type of magnetic superconductor is the one where the moment is itinerant. In itinerant electron systems long range order may be carried by the same electrons that become superconducting, leading to competition (sometime strong) between the two states. The recently discovered iron arsenic based superconductors appear to be one such example. The parent compounds (RFeAsO 1111 series, $\text{R}=\text{La, Ce, Pr, Nd, Sm or Gd}$, and AFe_2As_2 122 series, alkali earth $\text{A}=\text{Ca, Sr, Ba}$) are semimetals and show either closely spaced, or a simultaneous AF ordering and tetragonal to orthorhombic

(ortho) structural transition. With electron or hole doping, the magnetic and structural transitions are suppressed to low temperature and SC, with T_c up to 55 K¹², is induced. $\text{Ba}_{1-x}\text{K}_x\text{Fe}_2\text{As}_2$ ¹³ exhibits a maximum T_c of 37 K, or by substitution of transition metal for Fe, e.g. $\text{Ba}(\text{Fe}_{1-x}\text{Co}_x)_2\text{As}_2$, T_c can reach 22 K¹⁴⁻¹⁶ or for $\text{Sr}(\text{Fe}_{1-x}\text{Co}_x)_2\text{As}_2$, T_c can reach 18 K.¹⁷ Unlike the 1111 series for which the magnetic/structural transition was suggested to disappear abruptly prior to the emergence of SC, the 122 series show a gradual suppression of the AF/ortho transition, which coexists with SC for a range of dopings.^{15,16} For the Co doped Ba-122 series neutron scattering shows a suppression of the magnetic order parameter on entering the superconducting state, indicating strong coupling between AF and SC.^{15,18} In addition, both μSR ^{19,20} and ^{75}As NMR²¹ measurements unambiguously indicate that AF order is present in all of the sample volume when the sample is in the superconducting state, i.e. that the magnetic order and SC coexist homogeneously at the atomic scale. Whereas Fe-based AF coexists with SC and Fe based AF fluctuations may well be vital to FeAs based superconductors, a systematic study of effects of well defined, local magnetic moments on this SC is lacking. Starting from optimally Co-doped SrFe_2As_2 , we can have Eu^{2+} substituting for Sr^{2+} without introducing extra electrons/holes and assess the sensitivity of this SC to the large $J = S = 7/2$ local moment.

The Eu end compound, EuFe_2As_2 , exists as an isostructural member of the 122 series. Therefore a continuous substitution can be expected between EuFe_2As_2 and AFe_2As_2 . EuFe_2As_2 , in addition to the AF order of the iron sublattice at about 189 K, exhibits an A-type AF order of Eu^{2+} ions at 19 K.²² On suppression of the AF order of iron with pressure or Co doping²³⁻²⁴, the onset of SC was observed, which was then followed by a resistive reentrance attributed to the magnetic order of Eu^{2+} . Given the sensitivity of the 122 compounds to

strain/pressure^{25–30}, we choose SrFe_2As_2 as host, owing to the similar size of Sr^{2+} (118 pm) and Eu^{2+} (117 pm)³¹, so as to minimize the steric effects of the doping.

In order to perturb the SC of the Sr 122 phase by isoelectronic substitution of Eu and establish phase diagrams systematically using the same growth technique for Co and Eu doping, the phase diagram of $\text{Sr}(\text{Fe}_{1-x}\text{Co}_x)_2\text{As}_2$ as a function of Co substitution is constructed first. The optimal Co doping level of $x \sim 0.12$ is then kept the same across the whole range of Eu doping. We present the magnetic susceptibility, resistivity and heat capacity measurements on $\text{Sr}_{1-y}\text{Eu}_y(\text{Fe}_{1-x}\text{Co}_x)_2\text{As}_2$. Superconductivity of the optimally Co doped SrFe_2As_2 is suppressed gradually by Eu doping ($0 \leq y < 0.43$), crosses over a region with coexistence of SC and Eu based AF ($0.43 \leq y \leq 0.60$) with T_N increasing linearly with y . For $y \geq 0.65$, T_N cuts across the T_c line and SC suddenly disappears leaving just the Eu^{2+} , AF ordered state. An initial study of EuFe_2As_2 doped with both Sr and Co was recently published, but using samples with nominal doping values and focusing on the Eu-rich side.³² We will compare the results of our systematic study with Ref. 32 in the discussion section.

II. EXPERIMENT

Single crystal samples of both $\text{Sr}(\text{Fe}_{1-x}\text{Co}_x)_2\text{As}_2$ and $\text{Sr}_{1-y}\text{Eu}_y(\text{Fe}_{0.88}\text{Co}_{0.12})_2\text{As}_2$ were grown via a self flux method.^{16,33} The FeAs and CoAs precursors were first synthesized by solid state reaction. Elemental Sr and Eu were mixed with FeAs and CoAs in the stoichiometry of $1 : 4 - 4x : 4x$ and $1 - y : y : 3.44 : 0.56$ respectively in an alumina crucible and sealed into an amorphous silica tube. The sealed ampoule was heated to 1180 °C and then cooled slowly to 1000 °C; finally the excess liquid flux was decanted.³³ The as-grown crystals were annealed under a static Ar atmosphere at 500 °C for 24 hours (as discussed below in Section III).³⁴

Powder x-ray diffraction, with Si standard, was performed using a Rigaku Miniflex X-ray diffractometer with Cu $K\alpha$ radiation ($\lambda = 1.5418\text{\AA}$). The lattice parameters were refined by Rietica software.³⁵ Chemical composition was determined by wavelength dispersive x-ray spectroscopy (WDS) in a JEOL JXA-8200 electron microscope. The actual composition of the single crystals was taken as the average of 10 spots measured on the crystal and the error bar was taken as the standard deviation of the 10 values.

Magnetic susceptibility was measured in a Quantum Design MPMS, SQUID magnetometer. The in-plane AC resistivity was measured by a standard four-probe method using an LR-700 resistance bridge with an excitation of 60 μV on samples of typical size $3\text{ mm} \times 2\text{ mm} \times 0.2\text{ mm}$. Electrical contacts were made using Dupont 4929N silver paint. Heat capacity data were collected using a Quantum Design PPMS.

All the samples were found to slowly degrade in air.

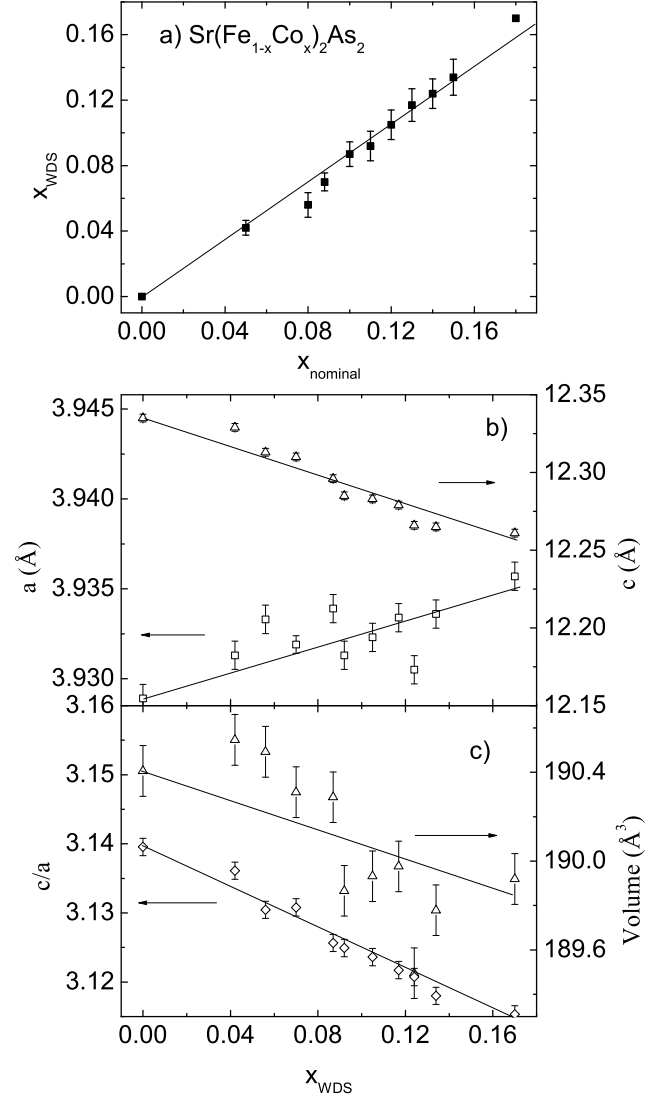


FIG. 1: Results of elemental analysis and lattice parameters determined on $\text{Sr}(\text{Fe}_{1-x}\text{Co}_x)_2\text{As}_2$. a) Measured Co concentration from WDS vs. nominal one; b-c) Lattice parameters, a , c , c/a and unit cell volume as a function of x_{WDS} .

Over a period of four months, a ferromagnetic background on the order of 10^{-2} emu/mol develops, although no obvious change in appearance of the crystal and no impurity phase in powder XRD pattern can be observed. Elemental analysis indicates significant presence of oxygen in the surface layer of the aged samples, implying the formation of oxides. In addition, the superconducting transition of the aged sample broadens and T_c decreases as measured by low field magnetization. Therefore all the measurements reported in this paper were performed shortly after the samples were prepared. It should be noted that whereas the Sr-based 122 compounds are known to be susceptible to chemical changes³⁶, as well as strain²⁷, we observed no sample quality change over time.

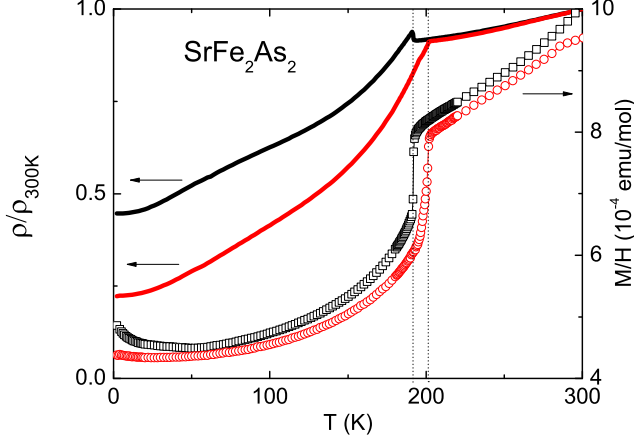


FIG. 2: The annealing effect for pure SrFe_2As_2 . As-grown sample (black), annealed sample (red)

in the well studied^{15,16} $\text{Ba}(\text{Fe}_{1-x}\text{Co}_x)_2\text{As}_2$ samples.

III. RESULTS AND DISCUSSIONS

1. $\text{Sr}(\text{Fe}_{1-x}\text{Co}_x)_2\text{As}_2$

The results of elemental analysis and lattice parameter determined from the powder X-ray measurements on $\text{Sr}(\text{Fe}_{1-x}\text{Co}_x)_2\text{As}_2$ are shown in Fig. 1. The nearly linear dependence in Fig. 1(a), with a slope of 0.94, indicates good agreement between the actual Co concentration, x_{WDS} , and the nominal concentration, x_{nominal} . The compositional spread over a wide area on the sample surface for each concentration is less than 0.02. These results demonstrate the relative homogeneity of the Co doping in the single crystal samples. Figures 1(b) and (c) show that the lattice parameters a and c , as well as the c/a ratio and unit cell volume as a function of x_{WDS} . The parameter c , and c/a , change linearly with x_{WDS} and the values are in good agreement with the previous report.¹⁷ By substitution of Co for Fe the lattice is changed more along c axis than in the ab plane. The lattice parameter c decreases by 0.6% (0.074 Å) for $x = 0.17$, whereas the lattice parameter a increases by only about 0.2% (0.007 Å). The random error of lattice parameter determined by our Miniflex X-ray diffractometer is about 0.02%, ~ 0.0008 Å for the a lattice parameter, which is about the same order as the average deviation from a linear variation ~ 0.0013 Å. Thus lattice parameters can be regarded to vary linearly with x_{WDS} , within experimental errors, in accordance with Vegard's law.

Annealing can have clear effect on samples and has been shown to remove extrinsic effects associated with strain induced defects.³⁴ As shown in Fig. 2, the magnetic/structural transition of pure SrFe_2As_2 is increased

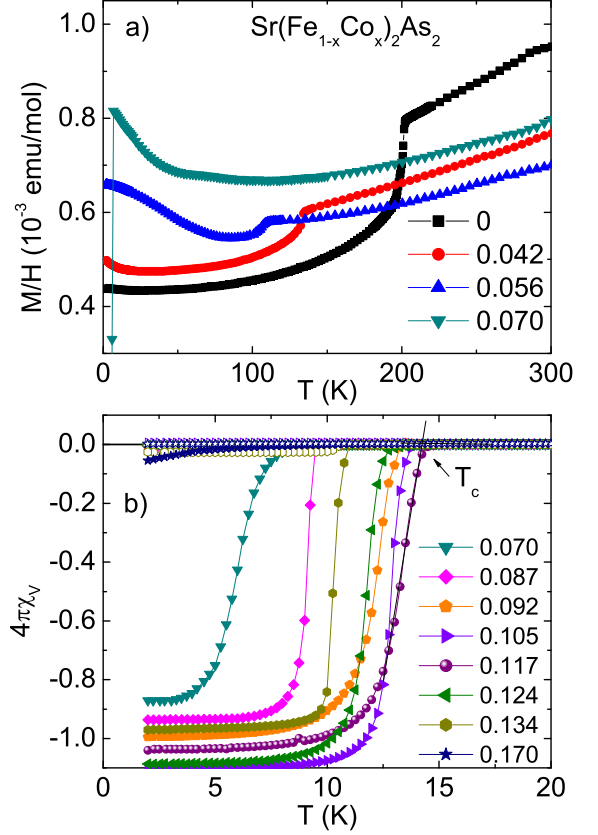


FIG. 3: a) Magnetic susceptibility as a function of temperature for $\text{Sr}(\text{Fe}_{1-x}\text{Co}_x)_2\text{As}_2$ single crystals taken at 10 kOe with $\mathbf{H} \parallel ab$; b) Low field (100 Oe) magnetic susceptibility. Field-cooled curves are shown in open symbols. T_c is inferred from the intersect of the steepest slope to the normal magnetic susceptibility.

from 192 K, for the as grown sample to 201 K, for the annealed sample, which is very close to the previous reported values for polycrystalline (205 K)³⁷ and Sn flux-grown single crystalline (198 K)³⁸ SrFe_2As_2 . Based on these observations, our samples are heat treated under the conditions described in Section II above.

The magnetic susceptibility for $\mathbf{H} \parallel ab$ of the $\text{Sr}(\text{Fe}_{1-x}\text{Co}_x)_2\text{As}_2$ series was measured in a magnetic field of 10 kOe for $x \leq 0.07$ (Fig. 3 (a)). The parent compound SrFe_2As_2 manifests a sharp drop at 201 K in magnetic susceptibility, due to the magnetic/structural transition.^{37,38} With increasing Co doping, this transition is suppressed to lower temperature and becomes undetectable for $x > 0.07$. For $0.07 \leq x \leq 0.17$, SC is induced and is manifested in low field ($H = 100$ Oe) zero-field-cooled (ZFC) and field-cooled (FC) measurements below 20 K (Fig. 3 (b)). The data are compared to $1/4\pi$ to give a rough estimate of the superconducting volume fraction. Although, as discussed in Ref. 39, the FC curves are routinely close to zero in these materials,

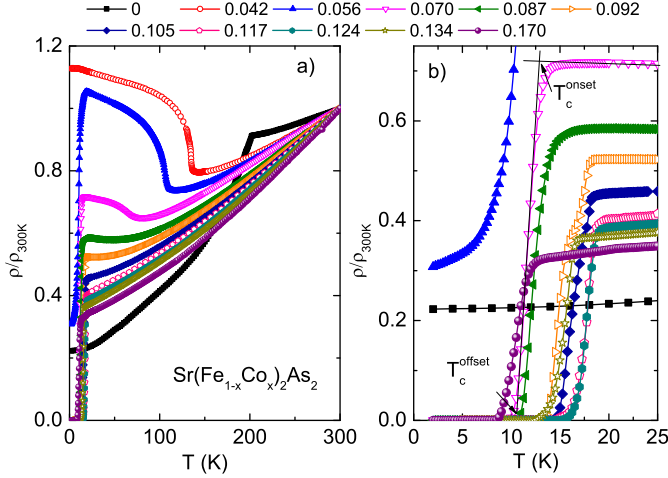


FIG. 4: a) Resistivity normalized to the room temperature value $\rho(T)/\rho(300K)$ for $\text{Sr}(\text{Fe}_{1-x}\text{Co}_x)_2\text{As}_2$ ($0 \leq x \leq 0.17$); b) Low temperature resistivity showing superconducting transition.

due to pinning or surface barrier effects, the ZFC curves approaching -1 suggest bulk SC. The superconducting transitions remain very sharp for $x \geq 0.07$, except for $x = 0.17$ which becomes broad and barely visible, consistent with a T_c reduced to a value close to our base temperature. The transition temperature increases from 7.4 K for $x = 0.07$, maximizes at 14.8 K for $x = 0.117$ and then diminishes to 5.7 K for $x = 0.17$.

Fig. 4(a) shows the temperature dependence of the electrical resistivity of $\text{Sr}(\text{Fe}_{1-x}\text{Co}_x)_2\text{As}_2$, normalized to the room temperature values. Similar to the case of $\text{Ba}(\text{Fe}_{1-x}\text{Co}_x)_2\text{As}_2$ series¹⁶, the magnetic/structural transition of $\text{Sr}(\text{Fe}_{1-x}\text{Co}_x)_2\text{As}_2$ manifests itself as a sudden drop for $x = 0$ and as an increase in resistivity for $x = 0.042 - 0.07$ and nearly disappears for $x = 0.087$. After the magnetic/structural transition is completely suppressed for $x \geq 0.092$, the series shows featureless, metallic temperature dependence. Fig. 4(b) shows an expanded view for low temperatures. At $x = 0.056$, a broad and incomplete superconducting transition is observed; zero resistance is only reached for $x \geq 0.07$, this agrees with the bulk SC observed in magnetic measurements.

In order to establish the phase diagram for the $\text{Sr}(\text{Fe}_{1-x}\text{Co}_x)_2\text{As}_2$ series, the transition temperatures were inferred in the same manner as used in Ref. 16. T_c from magnetic susceptibility is determined from the intersection of the steepest slope and the linear extrapolation of normal magnetic susceptibility, shown in Fig. 3 (b). Resistive onset and offset of T_c values are inferred from the intersects of the steepest slope with the normal state and zero resistance respectively, shown in Fig. 4 (b). $T_{M/S}$ is inferred from the peak of $d(M/H)/dT$ and $d[\rho/\rho(300K)]/dT$; data for $x = 0.056$ is shown in Fig. 5 as an example. It is argued by Gillett *et al*⁴⁰

that only a single, first-order-like, transition occurs in the heat capacity of $\text{Sr}(\text{Fe}_{1-x}\text{Co}_x)_2\text{As}_2$ with coincidence of magnetic and structural transitions. Our magnetization and resistance data also do not show a discernible splitting between T_M and T_S , Fig. 5, further supports this observation.

Based on our magnetization and electrical resistance measurements, the phase diagram of $\text{Sr}(\text{Fe}_{1-x}\text{Co}_x)_2\text{As}_2$ is mapped out in Fig. 6. A superconducting dome is found: SC is first stabilized for $x = 0.07$ at about 7.4 K, reaches a maximum T_c of ~ 14.5 K for $x = 0.117$, then decreases to 5.7 K for $x = 0.17$. Our phase diagram is in good agreement with earlier ones. The phase diagram for polycrystalline $\text{Sr}(\text{Fe}_{1-x}\text{Co}_x)_2\text{As}_2$ showed a complete suppression of magnetic/structural transition and appearance of SC at $x_{\text{nominal}} = 0.1$ with the highest T_c of 19 K.¹⁷ The difference between maximum T_c of the polycrystalline and our single crystalline samples is probably due to strain effect. As it has been demonstrated²⁵⁻³⁰, strain can affect Sr122 profoundly, especially when there is a high surface area to volume fraction (as in powders). Results consistent with our single crystal $\text{Sr}(\text{Fe}_{1-x}\text{Co}_x)_2\text{As}_2$ work, with highest $T_c \sim 13$ K were reported by Kasinathan *et al.*⁴¹ The more recent one based on self-flux grown single crystals, having larger density of data points, showed more clearly a coexistence of $T_{M/S}$ and SC transition for $x = 0.07 \sim 0.09$ and the superconducting dome with optimal T_c of 16 K at $x = 0.10$.⁴⁰ The differences between our phase diagram and the published ones, in terms of transition temperature and optimal doping concentration, may be associated with differences in both sample preparation and uncertainties of concentration. For our self-flux grown samples, we can choose Co concentration $x \sim 0.12$, with the highest T_c and suppressed AF/ortho transition as the starting point for our study of the effects of local moments of FeAs based superconductor via Eu substitution for Sr.

2. $\text{Sr}_{1-y}\text{Eu}_y(\text{Fe}_{1-x}\text{Co}_x)_2\text{As}_2$

For our $\text{Sr}_{1-y}\text{Eu}_y(\text{Fe}_{1-x}\text{Co}_x)_2\text{As}_2$ series, the Co concentration was kept at $x \sim 0.12$ and the series was doped by Eu for $0 \leq y \leq 1$. Fig. 7(a) shows the elemental analysis results for the actual Eu and Co concentrations as a function of nominal Eu concentration. The actual concentration of Eu agrees well with the nominal, with a slope of 1.03, and the Co concentration is essentially constant. The lattice parameters a , c and unit cell volume are plotted in Figs. 7(b) and (c). Compared to $\text{Sr}(\text{Fe}_{0.883}\text{Co}_{0.117})_2\text{As}_2$ ($a = 3.9334(2)$ Å, $c = 12.2790(2)$ Å), the smaller Eu^{2+} ion leads to a decrease in c axis by 2% (0.256 Å) and a decrease in a axis by 0.4% (0.014 Å). The small concentration error and linear dependence on x_{WDS} indicate a homogeneous substitution of Sr by Eu across the whole series.

The in-plane magnetic susceptibility of

TABLE I: Results of elemental analysis for $\text{Sr}_{1-y}\text{Eu}_y(\text{Fe}_{1-x}\text{Co}_x)_2\text{As}_2$ and the Eu^{2+} concentration inferred from high temperature magnetic susceptibility. The Curie-Weiss temperature θ_{CW} is compared with the AFM transition temperature T_N .

y_{nominal}	0.05	0.1	0.15	0.2	0.3	0.4	0.45	0.5	0.55	0.6	0.7	0.8	0.9	1
y_{WDS}	0.04	0.15	0.16	0.19	0.34	0.43	0.50	0.54	0.60	0.65	0.72	0.85	0.96	1
y_M	0.05	0.12	0.15	0.18	0.31	0.40	0.48	0.50	0.60	0.64	0.73	0.85	0.97	1
$\theta_{CW}(K)$	2.2	4.1	4.0	4.2	5.0	9.3	9.7	10.3	11.7	13.9	14.6	18.6	19.4	20.2
$T_N(K)$						3.5	4.5	5.5	6.3	8.0	9.5	11.8	14.3	16.8

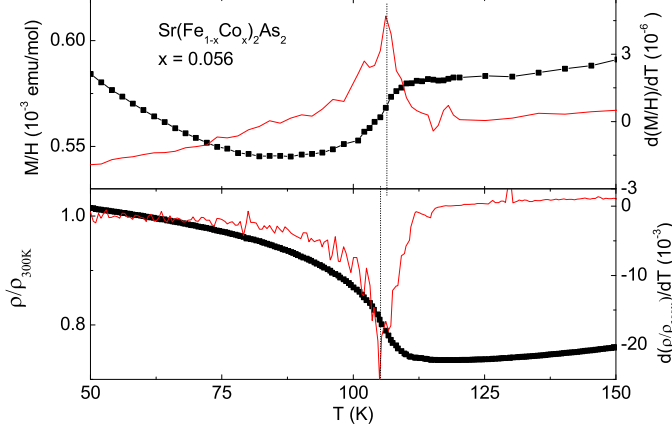


FIG. 5: Magnetic susceptibility, normalized resistivity and the temperature derivatives, single peak associated with simultaneous magnetic and structural transition.

$\text{Sr}_{1-y}\text{Eu}_y(\text{Fe}_{0.88}\text{Co}_{0.12})_2\text{As}_2$ is shown in Fig. 8. Both ZFC and FC curves are measured in a magnetic field of 100 Oe. The data clearly indicate that there are three regions of low temperature behavior across the series: i) $0 \leq y \leq 0.34$, SC is gradually suppressed by Eu doping but remains a simply identifiable transition; ii) $0.43 \leq y \leq 0.60$, in this intermediate range, the Curie-Weiss paramagnetic background due to Eu^{2+} moments gradually becomes large enough to shift the diamagnetic signal to positive values. In addition a second feature appears and as y increases it rises in temperature leading to a double-peak feature, which can be ascribed to the coexistence of SC and lower temperature AF associated with the Eu^{2+} sublattice. The upper transition shows a splitting between ZFC and FC curves consistent with SC. The lower transition of AF origin is present on both ZFC and FC curves at the same temperature, indicated by arrows. These transitions are further confirmed by heat capacity measurement as shown below; iii) $0.65 \leq y \leq 1$, clear AF transitions manifest as cusps and T_N continues to increase with Eu^{2+} doping up to 17 K for $y = 1$. It is worth noting that FC and ZFC curves collapse on each other for these higher y values, suggesting long range antiferromagnetic order, similar to EuFe_2As_2 ⁴², instead of other magnetic origin, e.g. spin glass or ferrimagnetic order.

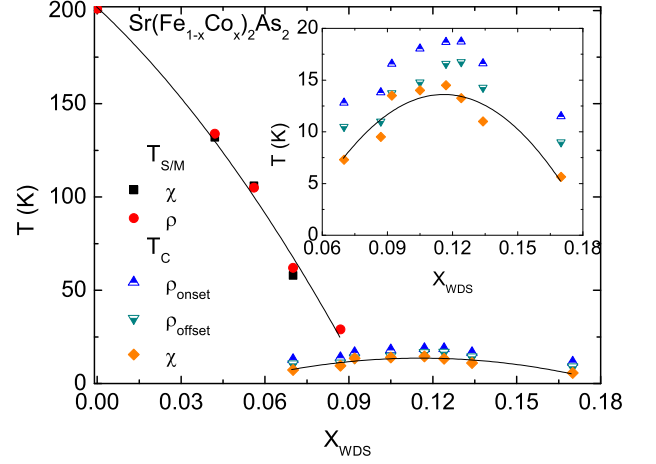


FIG. 6: Temperature and chemical composition phase diagram of $\text{Sr}(\text{Fe}_{1-x}\text{Co}_x)_2\text{As}_2$ single crystals for $0 \leq x \leq 0.17$. Lines are guide to the eye.

Fig. 9(a) shows $M(T)/H$ as a function of temperature data measured in various fields for $y = 1$. The cusp initially shifts to lower temperature with higher field and then becomes saturated paramagnetic-like for fields above 4 kOe. Neutron scattering experiments on pure EuFe_2As_2 revealed that the long range order of Eu^{2+} is of A-type AF, namely the Eu^{2+} moments are parallel in ab plane and antiparallel along c axis with an ordering wavevector of $k = (0, 0, 1)$.⁴³ Therefore the meta-magnetic transition for $y = 1$ is most likely due to the spin flip along the field direction between Eu^{2+} layers, similar to EuFe_2As_2 .⁴⁴ Our results are in good agreement with the reported magnetic field dependence of M/H for $\text{EuFe}_{1.715}\text{Co}_{0.285}\text{As}_2$, where meta-magnetic transition occurs at a lower field of 3.5 kOe than that of pure EuFe_2As_2 (8.5 kOe).⁴⁴ Because of this meta-magnetic transition, the series for $y \geq 0.43$ all show similar field dependence (Fig. 9(b)), i.e. the slope of magnetization changes around 4 kOe and shows a saturation moment of $\sim 7\mu_B/\text{Eu}^{2+}$ in high field. For $y = 0.43$ and 0.50, diamagnetic contribution of SC can be seen below 500 Oe. Given the meta-magnetic transition, the AF transition temperature T_N was inferred from the cusp of $d(\chi T)/dT$ measured in $H = 100$ Oe.⁴⁵

In Fig. 9(c) we examine the high temperature behavior

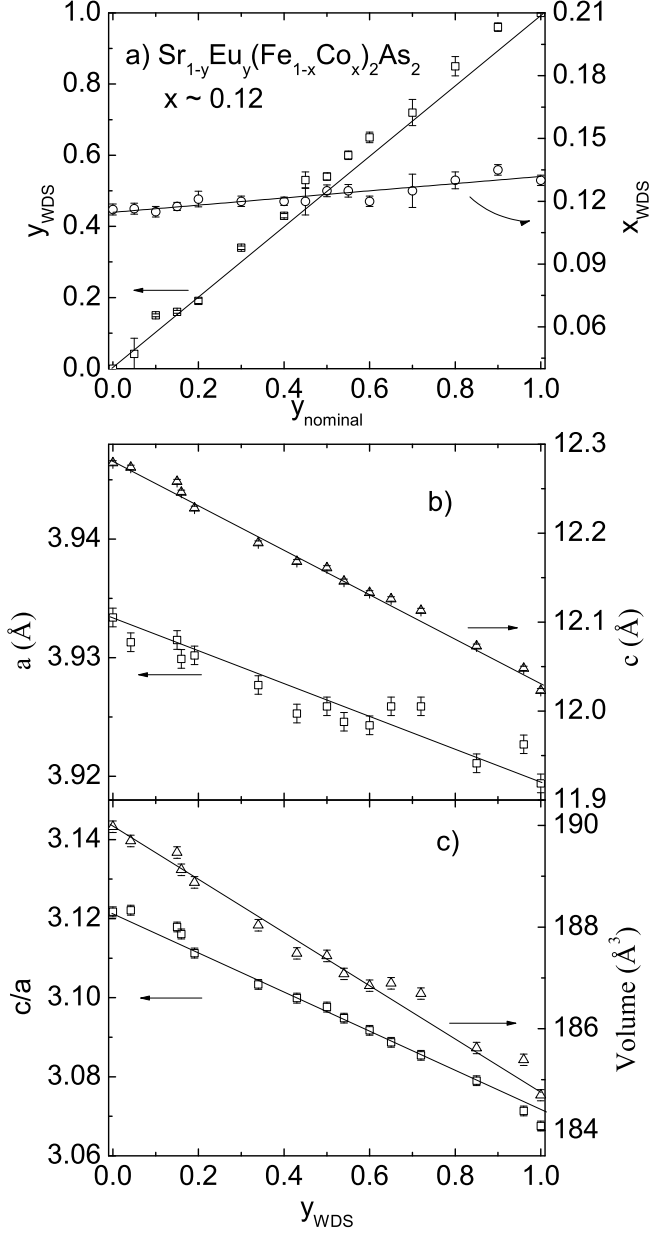


FIG. 7: a) Elemental analysis of $\text{Sr}_{1-y}\text{Eu}_y(\text{Fe}_{0.88}\text{Co}_{0.12})_2\text{As}_2$; b)-c) Lattice parameters, a , c and c/a , as well as unit cell volume.

ior of the magnetic susceptibility. Since the Hund's rule ground state for Eu^{2+} is the same as Gd^{3+} ($7/2S$), there is no spin-orbital coupling and thus the crystal field effect is absent and well defined magnetic moments of Eu^{2+} exhibiting Curie-Weiss law at high temperatures are expected. We are able to estimate the concentration of Eu^{2+} from magnetic measurements by assuming each Eu^{2+} carries an effective magnetic moment of $7.94\mu_B$. The magnetic background of $\text{Sr}(\text{Fe}_{0.883}\text{Co}_{0.117})_2\text{As}_2$ in a magnetic field of 10 kOe is subtracted from all the datasets and the inverse magnetic susceptibility normal-

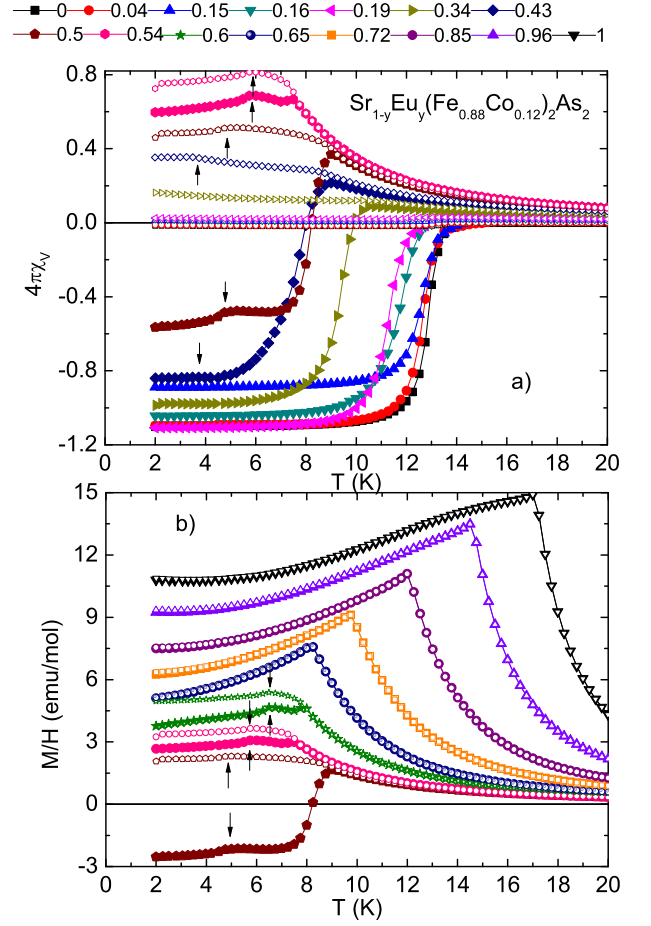


FIG. 8: Magnetic susceptibility of $\text{Sr}_{1-y}\text{Eu}_y(\text{Fe}_{0.88}\text{Co}_{0.12})_2\text{As}_2$ single crystals taken for 100 Oe magnetic field applied within the ab plane. Solid symbols denote ZFC data and open symbols denote FC data. Arrows indicate the AF transitions, which are consistent for both ZFC and FC curves.

ized to a fitted Eu concentration y_M is plotted in Fig. 9(c) as a function of temperature. The magnetic susceptibility above 100 K is fitted by the Curie-Weiss law:

$$\chi(T) = \frac{y_M N \mu(Eu^{2+})^2}{3k_B(T - \theta_{CW})} = \frac{7.94^2 y_M}{8(T - \theta_{CW})} [\text{emu/mol}]$$

where N is Avogadro constant, k_B is the Boltzmann constant and θ_{CW} is Curie-Weiss temperature. As can be seen in Table I, y_{WDS} and y_M agree well with each other and follow the same trend with the nominal concentration. The positive Curie-Weiss temperature is consistent with an overall predisposition to ferromagnetic coupling between Eu^{2+} moments, at least in the magnetic field of 10 kOe.

The low temperature ($T < 20\text{K}$) heat capacity divided by temperature, C_p/T , vs T of $\text{Sr}_{1-y}\text{Eu}_y(\text{Fe}_{0.88}\text{Co}_{0.12})_2\text{As}_2$ is presented in Fig. 10(a). A very pronounced discontinuity can be seen for $0.43 \leq$

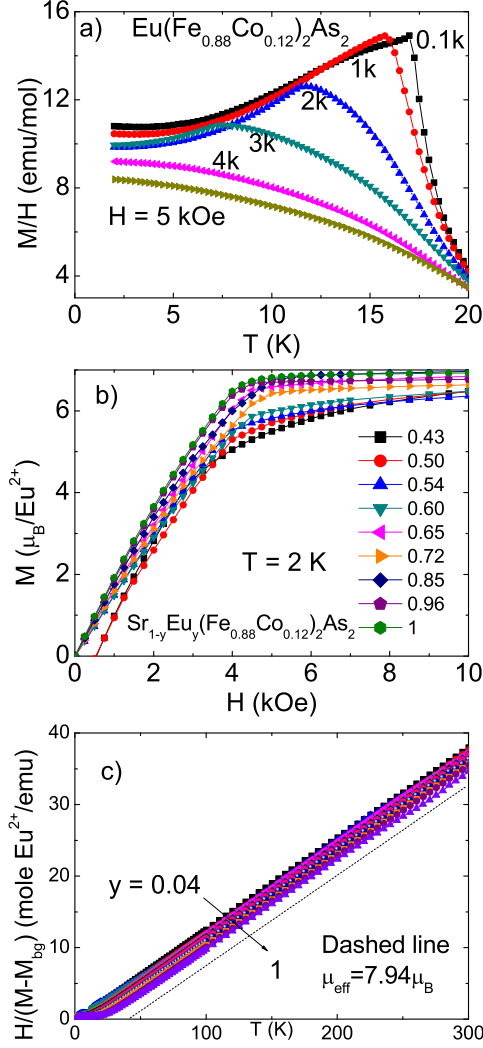


FIG. 9: a) Field dependence of the temperature dependent magnetization divided by applied field for $y = 1$ for $H \parallel ab$ plane; b) $M(H)$ normalized by y_{WDS} ; c) Inverse magnetic susceptibility, $H/(M-M_{bg})$ normalized by the actual Eu^{2+} concentration y_{WDS} .

$y \leq 1$. The transition temperature T_N , defined by this discontinuity, decreases with decreasing Eu^{2+} concentration and is in excellent agreement with the cusp of $d(\chi T)/dT$ of magnetic susceptibility. These data confirm that AF is the lower transition in the intermediate range $0.43 \leq y \leq 0.60$. For the $y = 0.34$ data this discontinuity appears to be at or just below our base temperature of 2.0 K. For $y < 0.34$ the complete transition can not be detected. It is worth noting that the low temperature C_p/T below 5 K for $0.65 \leq y \leq 1$ show a linear dependence on T , i.e. $C \propto T^2$. This temperature dependence of heat capacity is consistent with the low temperature AF magnon excitations of a two dimensional magnetic

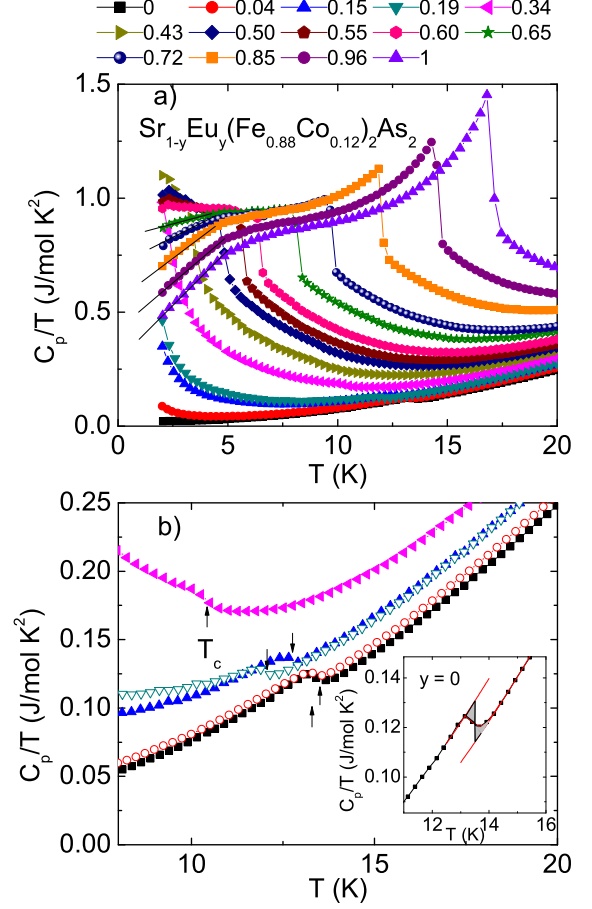


FIG. 10: a) C_p/T vs. T of $\text{Sr}_{1-y}\text{Eu}_y(\text{Fe}_{1-x}\text{Co}_x)_2\text{As}_2$, solid line indicates $C_p \sim T^2$ for a FM magnon contribution; b) an expanded view for $0 \leq y \leq 0.19$ showing a SC jump, T_c is indicated by arrows. Inset shows the isoentropic reconstruction of the superconducting transition of C_p/T .

lattice.⁴⁶

Figure 10(b) shows that starting from the low y side, SC can be identified as a weak jump for $0 \leq y \leq 0.19$, but becomes hard to detect for $y > 0.34$ because of the large background associated with the AF transition. Fig. 10(b) inset shows a representative heat capacity jump for $y = 0$. The SC transition temperature T_c is inferred by isoentropic construction, i.e. the two shaded areas have the same size. For $y = 0.34$, T_c is taken as the middle point of the jump.

Figure 11 shows the temperature dependence of the normalized resistivity of $\text{Sr}_{1-y}\text{Eu}_y(\text{Fe}_{0.88}\text{Co}_{0.12})_2\text{As}_2$. Given the Co-doping level (near optimal), it is not surprising that the series remains metallic and featureless above 20 K. In Fig. 11(b) it can be seen that superconducting transition temperature is gradually lowered by Eu^{2+} doping for $0 \leq y \leq 0.60$. The transition becomes broader for $y > 0.19$, e.g. ΔT is 4 K for $y = 0$ and 6 K for $y = 0.5$. This wide transition is similarly observed in

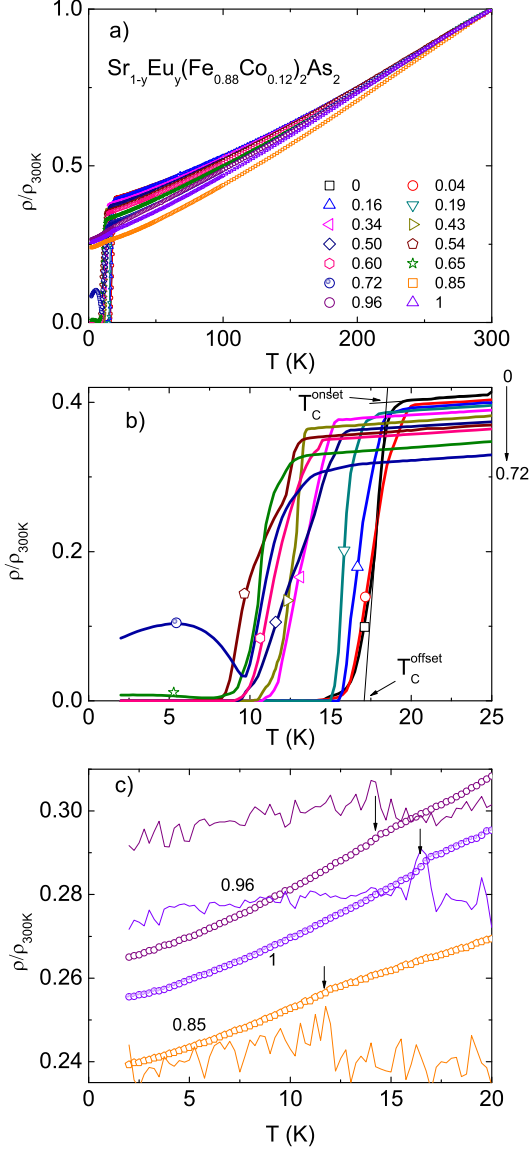


FIG. 11: a) Normalized electrical resistivity of $\text{Sr}_{1-y}\text{Eu}_y(\text{Fe}_{0.88}\text{Co}_{0.12})_2\text{As}_2$; b) Low temperature data showing the superconducting transition; c) For $0.85 \leq y \leq 1$, the loss of spin scattering around T_N , solid lines are the temperature derivatives.

Ni doped SrFe_2As_2 .³⁴ For $y = 0.65$ and 0.72 , a resistivity reentrance is observed as a broad peak below a local minimum in resistivity at 7.8 and 9.8 K respectively. The minimum coincides with the AF order temperature measured by magnetic susceptibility and heat capacity, indicating that the bulk SC transition is interrupted by AF order. Such incomplete resistive transitions have been observed in $\text{Sr}_{0.3}\text{Eu}_{0.7}(\text{Fe}_{0.86}\text{Co}_{0.14})_2\text{As}_2$ and EuFe_2As_2 under pressure,^{23,32}

The superconducting transition temperature, T_c , is inferred in the same way as in Fig. 4. For $y = 0.65$ and

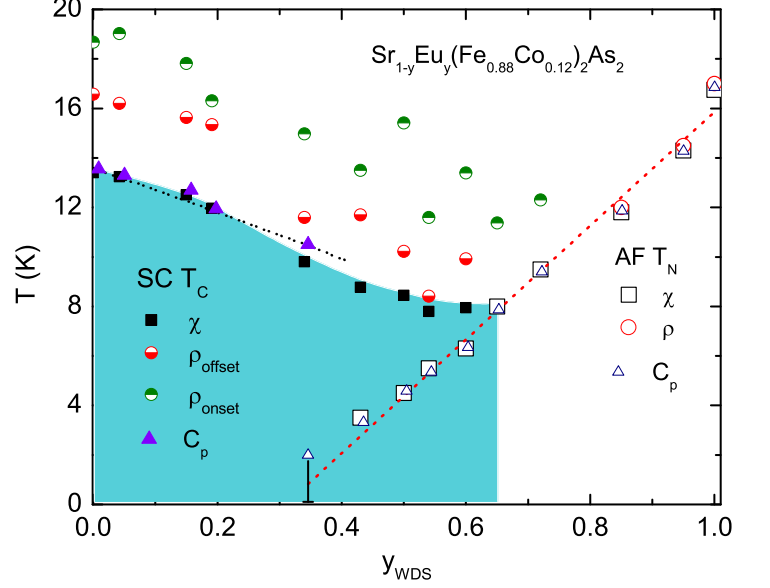


FIG. 12: $T - y$ phase diagram of $\text{Sr}_{1-y}\text{Eu}_y(\text{Fe}_{0.88}\text{Co}_{0.12})_2\text{As}_2$ single crystals. Black dashed line is the fit to AG theory. Red dashed line highlights $T_N(y)$ and is just a guide to the eye. Blue area is the superconducting region.

0.72, only T_c^{onset} is extracted. For $0.85 \leq y \leq 1$, Fig. 11(c), the series remains a normal metal and manifests a very small change in slope at T_N (corresponding to the peak in $d[\rho/\rho(300K)]/dT$), due to the loss of spin disorder scattering. We must note that the change in resistivity at T_N is very small, even smaller than that of EuFe_2As_2 .⁴² It implies very weak coupling between Eu^{2+} moments and conduction electrons. A recent detailed transport studies of EuFe_2As_2 under high pressure showed that electron scattering due to Eu^{2+} has minor contribution to both resistivity and Hall effect, thus consistent with our conclusion.⁴⁷

3. Analysis and discussion

Based on the transport and thermodynamic measurements, a phase diagram as a function of Eu doping can be constructed and is shown in Fig. 12. Starting from the Eu-rich side of the phase diagram, we can see that T_N decreases with decreasing Eu content and crosses through the T_c line, near $y \sim 0.60$, without any resolvable change in slope (dT_N/dy). This is fairly standard behavior for an intermetallic compound with a local moment antiferromagnetic phase transition that is being reduced via site dilution with a non-magnetic ion (i.e. Sr^{2+} for Eu^{2+}).^{11,48} Starting from the Sr-rich side of the phase diagram we can see that when Eu^{2+} is a paramagnetic impurity, it suppresses SC monotonically, but rather weakly. The weakness of the paramagnetic Eu^{2+}

as a pair breaker is not unexpected, given the rather weak coupling of the Eu^{2+} moments to the conduction electrons, as most clearly manifested by the small loss of spin-disorder scattering seen in Fig. 11(c). The suppression of T_c by magnetic impurities in a nonmagnetic superconductor has been discussed by Abrikosov and Gor'kov.¹ The fit to AG theory for data $0 \leq y \leq 0.34$ gives a critical concentration $y_c = 1.08$, implying SC could survive in $\text{Eu}(\text{Fe}_{0.88}\text{Co}_{0.12})_2\text{As}_2$ if the Eu^{2+} sublattice were to remain in the disordered paramagnetic state (*which it does not*). For $0.43 \leq y \leq 0.60$, both SC and AF states are clearly detected. As long as $T_c > T_N$, the advent of AF order does not lead to any re-entrance or other clear features in the $T - y_{WDS}$ phase diagram. This is in agreement with early findings that EuFe_2As_2 becomes a bulk superconductor with $T_c \sim 30$ K and SC coexists with AFM order with $T_N \sim 20$ K.⁴⁹ The remarkable feature revealed in Fig. 12 is the sudden disappearance of bulk SC when the T_N line intercepts the T_c line. Superconductivity, as defined by a $\rho = 0$ state, suddenly disappears for $y \geq 0.65$. This sudden truncation of the superconducting region is quite remarkable and demands further analysis.

As has been shown in this work and discussed before^{27,34}, the resistivity data associated with pure and doped SrFe_2As_2 samples is complicated, manifesting superconducting transition temperatures that appear to be higher than those determined by bulk, thermodynamic measurements such as magnetic susceptibility and specific heat. On the other hand, in both figures 6 and 12 the superconducting transition inferred from resistivity roughly tracks those inferred from magnetization and specific heat (in Fig. 12 even the T_c data inferred from onset criterion drop by a similar amount as the T_c values inferred from thermodynamic data, just with an offset by a few degrees). This is consistent with the idea that a small portion of the sample has an enhance T_c associated with some strain/damage. Similar difference of T_c between that inferred from resistivity and magnetic susceptibility, as well as transition width ΔT_c , were observed in Fig. 6 and in $\text{Sr}(\text{Fe}_{1-x}\text{Ni}_x)_2\text{As}_2$ ³⁴ This being said, the absence of any hint of superconducting drop in the $y > 0.72$ data (Fig. 11 (c)) is a conclusive evidence that there is not even trace superconductivity in these samples. For the $y = 0.65$ and 0.72 samples there appears to be an onset of filamentary superconductivity that is interrupted by the bulk AF.

In comparison to Ref. 32, whereas the above discussion and data show that AF appears to be very detrimental to the formation of the superconducting state when $T_N > T_c$, there is no evidence of the AF leading to dramatic re-entrance of the normal state when $T_N < T_c$ (i.e. for $y \leq 0.60$). The resistivity data, as well as the susceptibility data do not show any feature that can be associated with the re-establishment of the normal state below the T_N line as it cuts under the superconducting state.

These observations have several implications and also suggest several directions for future research. First, al-

though dilute, paramagnetic, Eu^{2+} only weakly suppresses SC, antiferromagnetically ordered Eu^{2+} appears to prevent its formation. As has been the case for other magnetic superconductors, specifically the $\text{RNi}_2\text{B}_2\text{C}$ materials¹¹, a dramatic difference in the effects of local moments on SC can be observed when comparing disordered, single ions in paramagnetic state, and an antiferromagnetically ordered sublattice. In the case of $(\text{Ho}_{1-x}\text{Dy}_x)\text{Ni}_2\text{B}_2\text{C}$ ^{11,50} as T_c crosses from above T_N to below it, the cause of pair breaking changes from spin-flip scattering off of single impurities to interactions with magnetic excitations of the order state. In the case of $\text{Sr}_{1-y}\text{Eu}_y(\text{Fe}_{0.88}\text{Co}_{0.12})_2\text{As}_2$ the sudden loss of superconductivity as T_N rises above T_c implies that somehow long range antiferromagnetic order of the Eu sublattice strongly suppresses (or removes) necessary ingredients for the establishment of the superconducting state. If antiferromagnetic fluctuations of the Fe-sublattice (associated with the $k = (1, 0, 1)$ ordering⁵¹) are associated with the pairing in the superconducting state, then long range order of the large ($J = S = 7/2$) Eu sublattice with an ordering wave vector of $k = (1, 0, 0)$ could easily be related to a dramatic change in the Fe sublattice fluctuation spectrum. Such a dramatic change in the fluctuations could easily be the suppressed, missing ingredient for superconductivity invoked above. So, unlike $\text{DyNi}_2\text{B}_2\text{C}$, which apparently requires antiferromagnetic ordering of the Dy sublattice to suppress pair breaking of the individual Dy moments¹¹, $\text{Sr}_{1-y}\text{Eu}_y(\text{Fe}_{0.88}\text{Co}_{0.12})_2\text{As}_2$ requires the Eu sublattice to remain in the disordered, paramagnetic state in order to establish the FeAs-based superconducting state.

Although this hypothesis readily explains the sudden loss of SC when $T_N > T_c$, it also would imply that the SC state below T_N , when $T_N < T_c$, should be modified; although figures 8, 11, and 12 show that there is no effect of T_N on the low field magnetization and zero field resistivity when $T_N < T_c$, it is reasonable to anticipate that there will be changes in other superconducting parameters such as the superfluid density and penetration depth.

IV. CONCLUSIONS

Transport and thermodynamic measurements were performed on $\text{Sr}(\text{Fe}_{1-x}\text{Co}_x)_2\text{As}_2$ and $\text{Sr}_{1-y}\text{Eu}_y(\text{Fe}_{0.88}\text{Co}_{0.12})_2\text{As}_2$ single crystals. A superconducting dome is identified in $\text{Sr}(\text{Fe}_{1-x}\text{Co}_x)_2\text{As}_2$ as a function of Co doping and the optimal Co concentration is determined to be $x \sim 0.12$. The SC of the optimal Co doping is gradually suppressed by paramagnetic Eu^{2+} following AG theory and found to coexist with AF of Eu^{2+} for $0.43 \leq y \leq 0.60$. For higher Eu^{2+} doping, bulk SC disappears suddenly when $T_N > T_c$. We speculate that the long range order of Eu^{2+} sublattice is coupled to the AF fluctuations of Fe sublattice and the suppression of the Fe fluctuations required for FeAs-based SC is

what gives rise to the abrupt loss of bulk SC when T_N surpasses T_c .

V. ACKNOWLEDGEMENTS

The authors acknowledge Alex Thaler for experimental assistance, Cedomir Petrovic, Jörg Schmalian and Rafael M. Fernandes for helpful discussions. This work was carried out at the Iowa State University and sup-

ported by the AFOSR-MURI grant #FA9550-09-1-0603 (Rongwei Hu, Paul C. Canfield). Part of this work was performed at Ames Laboratory, US DOE, under contract # DE-AC02-07CH 11358 (Sergey L. Bud'ko, Warren E. Straszheim and Paul C. Canfield). Sergey L. Bud'ko was also partially supported by the State of Iowa through the Iowa State University.

-
- ¹ A.A. Abrikosov, L.P. Gor'kov, Sov. Phys. JETP **16**, 1575 (1962)
 - ² B.T. Matthias, H. Suhl, E. Corenzwit, Phys. Rev. Lett, **1**, 92 (1958)
 - ³ Matthias B T, Suhl H and Corenzwit E, Phys. Rev. Lett. **1** 449 (1958)
 - ⁴ L. J. Williams, W. R. Decker, and D. K. Finnemore, Phys. Rev. B **2**, 1287 (1970)
 - ⁵ K. Machida, Appl. Phys. A **35**, 193 (1984)
 - ⁶ K-H Müller and V N Narozhnyi, Rep. Prog. Phys. **64** 943 (2001).
 - ⁷ L. C. Gupta, Advances in Physics, **55**, 691 (2006).
 - ⁸ O Ø. Fischer, M. B. Maple, Superconductivity in Ternary Compounds I, Structural, Electronic and Lattice Properties, Springer (1982).
 - ⁹ K. Buschow, E. Wohlfarth, Ferromagnetic Materials, Chap. 6, Elsevier, Amsterdam (1990).
 - ¹⁰ Charles P. Poole Jr., Paul. C. Canfield, Arthur P. Ramirez, Handbook of superconductivity, Pages 71-108 (2000).
 - ¹¹ Paul C. Canfield, Peter L. Gammel and David J. Bishop, Physics Today, **51**, 40 (1998).
 - ¹² Y. Kamihara, T. Watanabe, M. Hirano, and H. Hosono, J. Am. Chem. Soc. **130**, 3296 (2008).
 - ¹³ M. Rotter, M. Tegel, and D. Johrendt, Phys. Rev. Lett. **101**, 107006 (2008).
 - ¹⁴ A. S. Sefat, R. Jin, M. A. McGuire, B. C. Sales, D. J. Singh, and D. Mandrus, Phys. Rev. Lett. **101**, 117004 (2008).
 - ¹⁵ Paul C. Canfield and Sergey L. Bud'ko, Annual Review of Condensed Matter Physics, **1**, 27 (2010).
 - ¹⁶ N. Ni, M. E. Tillman, J.-Q. Yan, A. Kracher, S. T. Hannahs, S. L. Bud'ko, and P. C. Canfield, Phys. Rev. B **78**, 214515 (2008).
 - ¹⁷ A. Leithe-Jasper, W. Schnelle, C. Geibel, and H. Rosner, Phys. Rev. Lett. **101**, 207004 (2008).
 - ¹⁸ D. K. Pratt, W. Tian, A. Kreyssig, J. L. Zarestky, S. Nandi, N. Ni, S. L. Bud'ko, P. C. Canfield, A. I. Goldman, and R. J. McQueeney, Phys. Rev. Lett. **103**, 087001 (2009).
 - ¹⁹ C Bernhard, A J Drew, L Schulz, V K Malik, M Rossle, Ch Niedermayer, Th Wolf, G D Varma, G Mu, H-H Wen, H Liu, G Wu and X H Chen, New J. Phys., **11**, 055050 (2009).
 - ²⁰ R. Khasanov, A. Maisuradze, H. Maeter, A. Kwadrin, H. Luetkens, A. Amato, W. Schnelle, H. Rosner, A. Leithe-Jasper, and H.-H. Klauss, Phys. Rev. Lett. **103**, 067010 (2009).
 - ²¹ Y. Laplace, J. Bobroff, F. Rullier-Albenque, D. Colson, and A. Forget, Phys. Rev. B **80**, 140501 (2009).
 - ²² H. S. Jeevan, Z. Hossain, Deepa Kasinathan, H. Rosner, C. Geibel and P. Gegenwart, Phys. Rev. B **78**, 052502 (2008).
 - ²³ C. F. Miclea, M. Nicklas, H. S. Jeevan, D. Kasinathan, Z. Hossain, H. Rosner, P. Gegenwart, C. Geibel and P. Steglich, Phys. Rev. B **79**, 212509 (2009).
 - ²⁴ M. Nicklas, M. Kumar, E. Lengyel, W. Schnelle, A. Leithe-Jasper, arXiv:1006.3471v1 (2010).
 - ²⁵ Milton S. Torikachvili, Sergey L. Bud'ko, Ni Ni, Paul C. Canfield, Phys. Rev. Lett. **101**, 057006 (2008).
 - ²⁶ Patricia L. Alireza, Y. T. Chris Ko, Jack Gillett, Chiara M. Petrone, Jacqueline M. Cole, Gilbert G. Lonzarich, Suchitra E. Sebastian, J. Phys.: Condens. Matter **21**, 012208 (2009).
 - ²⁷ S. R. Saha, N. P. Butch, K. Kirshenbaum, and Johnpierre Paglione, Phys. Rev. Lett. **103**, 037005 (2009).
 - ²⁸ E. Colombier, S. L. Bud'ko, N. Ni, P. C. Canfield, Phys. Rev. B **79**, 224518 (2009).
 - ²⁹ S. Kawasaki, T. Tabuchi, X. F. Wang, X. H. Chen and Guo-qing Zheng, Supercond. Sci. Technol. **23**, 054004 (2010).
 - ³⁰ Tuson Park, Eunsung Park, Hanoh Lee, T. Klimczuk, E. D. Bauer, F. Ronning and J. D. Thompson, J. Phys.: Condens. Matter **20** 322204 (2008).
 - ³¹ R. D. Shannon, Acta Cryst., A32 751 (1976).
 - ³² Y He, T Wu, G Wu, Q J Zheng, Y Z Liu, H. Chen, J J Ying, R H Liu, X F Wang, Y L Xie, Y J Yan, J K Dong, S Y Li and X H Chen, J. Phys.: Condens. Matter **22**, 235701 (2010).
 - ³³ P. C. Canfield and Z. Fisk, Philos. Mag. B **65**, 1117 (1992).
 - ³⁴ S. R. Saha, N. P. Butch, K. Kirshenbaum, and Johnpierre Paglione, Phys. Rev. B **79**, 224519 (2009).
 - ³⁵ Hunter B., "Rietica - A visual Rietveld program", International Union of Crystallography Commission on Powder Diffraction Newsletter No. 20, (Summer) <http://www.rietica.org> (1998).
 - ³⁶ Hidenori Hiramatsu, Takayoshi Katase, Toshio Kamiya, Masahiro Hirano, and Hideo Hosono, Phys. Rev. B **80**, 052501 (2009).
 - ³⁷ A. Jesche, N. Caroca-Canales, H. Rosner, H. Borrmann, A. Ormeci D. Kasinathan, H. H. Klauss, H. Luetkens, R. Khasanov, A. Amato, A. Hoser, K. Kaneko, C. Krellner, and C. Geibel, Phys. Rev. B **78**, 180504 (2008).
 - ³⁸ J.-Q. Yan, A. Kreyssig, S. Nandi, N. Ni, S. L. Bud'ko, A. Kracher, R. J. McQueeney, R. W. McCallum, T. A. Lograsso, A. I. Goldman, and P. C. Canfield, Phys. Rev. B **78**, 024516 (2008).
 - ³⁹ R. Prozorov, M. A. Tanatar, Bing Shen, Peng Cheng, Hai-Hu Wen, S. L. Bud'ko, P. C. Canfield, Phys. Rev. B **82**,

- 180513(R) (2010).
- ⁴⁰ Jack Gillett, Sitikantha D. Das, Paul Syers, Alison K. T. Ming, Jose I. Espeso, Chiara M. Petrone, and Suchitra E. Sebastian, arXiv:1005.1330 (2010).
 - ⁴¹ Deepa Kasinathan, Alim Ormeci, Katrin Koch, Ulrich Burkhardt, Walter Schnelle, Andreas Leithe-Jasper and Helge Rosner, New J. Phys. **11** 025023 (2009).
 - ⁴² Zhi Ren, Zengwei Zhu, Shuai Jiang, Xiangfan Xu, Qian Tao, Cao Wang, Chunmu Feng, Guanghan Cao, and Zhu'an Xu, Phys. Rev. B **78**, 052501 (2008).
 - ⁴³ Y. Xiao, Y. Su, M. Meven, R. Mittal, C. M. N. Kumar, T. Chatterji, S. Price, J. Persson, N. Kumar, S. K. Dhar, A. Thamizhavel, and Th. Brueckel, Phys. Rev. B **80**, 174424 (2009).
 - ⁴⁴ Shuai Jiang, Yongkang Luo, Zhi Ren, Zengwei Zhu, Cao Wang, Xiangfan Xu, Qian Tao, Guanghan Cao and Zhu'an Xu, New Journal of Physics **11**, 025007 (2009).
 - ⁴⁵ M. E. Fisher, Phil. Mag., **7**, 1731 (1962).
 - ⁴⁶ L. J. de Jongh, A. R. Miedema, Adv. Phys., **23**, 1 (1974).
 - ⁴⁷ Taichi Terashima, Nobuyuki Kurita, Akiko Kikkawa, Hiroyuki S. Suzuki, Takehiko Matsumoto, Keizo Murata, and Shinya Uji, J. Phys. Soc. Jpn. **79**, 103706 (2010).
 - ⁴⁸ T. A. Wiener, I. R. Fisher, S. L. Bud'ko, A. Kracher, and P. C. Canfield, Phys. Rev. B **62**, 15056 (2000).
 - ⁴⁹ Taichi Terashima, Motoi Kimata, Hidetaka Satsukawa, Atsushi Harada, Kaori Hazama, Shinya Uji, Hiroyuki S. Suzuki, Takehiko Matsumoto, and Keizo Murata, J. Phys. Soc. Jpn. **78** 083701 (2009).
 - ⁵⁰ B. K. Cho, P. C. Canfield, D. C. Johnston, Phys. Rev. Lett., **77**, 163 (1996).
 - ⁵¹ J. Zhao, W. Ratcliff, J. W. Lynn, G. F. Chen, J. L. Luo, N. L. Wang, J. P. Hu, and P. C. Dai, Phys. Rev. B **78**, 140504 (2008).